

Toward a high-fidelity model for the identification of underground gas flow regimes resulting from buried pipeline releases

Ola Srour^a, Konstantinos E. Kakosimos^{a,b,*}, Luc N. Vechot^a

^a Department of Chemical Engineering and Mary Kay O'Connor Process Safety Center Qatar, Texas A&M University at Qatar, Doha, Qatar

^b Aerosol & Particle Technology Laboratory, Chemical Process & Energy Resources Institute, Centre for Research & Technology Hellas (APTL/CPERI/CERTH), Greece

ARTICLE INFO

Keywords:

Leak
Buried pipeline
Computational fluid dynamics
Eulerian model
Risk assessment

ABSTRACT

The quantitative characterization of underground transport phenomena remains challenging due to the complex behavior of the gas movement in soil. Conversely, this inhibits the accurate prediction of the risk arising from the underground transport of hazardous materials. This work proposed and qualitatively evaluated a computational model that spans a wide range of underground gas flow regimes, ranging from gas migration, to ground uplift, and crater formation, depending on the release characteristics. The model followed the multiphase Eulerian approach and adopted the standard $k-\omega$ turbulence model and the kinetic theory of granular flow for the ground description with the Syamlal-O'Brien granular viscosity expression. The model's optimum configuration was checked against experimental data using a new mechanistic approach to link the qualitative observations with quantitative model outputs. The effect of pipeline pressure, burial depth, and release orientation on the regime was studied and the outcomes were utilized to enhance a literature nomograph for the flow regime identification. Emphasis was given to fill in the literature gaps and improve the delineation of the boundaries between the regimes rather than deriving specific quantities. The resulted nomograph is a cost-effective screening tool to identify the regime and select among the available strategies of risk assessment.

1. Introduction

Buried pipelines are essential transmitters of natural gas, which worldwide consumption is expected to increase from 113 trillion cubic feet (Tcf) in 2010 to 185 Tcf in 2040 (Briefing, 2013). However, these pipelines are prone to leaks due to the operational and surrounding conditions that alter the state of the pipeline. In the USA, around 4000 gas pipeline failures have been reported between 2002 and 2016, accompanied with an estimated US\$ 2.7 billion worth of damages (Zakikhani et al., 2020). Such failures can lead to disastrous incidents, causing significant losses in terms of life, asset and environment, as demonstrated by the 2004 buried pipeline gas leak in Ghislenghien, Belgium (Biezma et al., 2020) that caused 24 fatalities, 132 injuries and very significant economic losses. Hence, it is crucial to understand the phenomena associated to underground gas releases in order to control the risks of such events.

The consequences of an underground gas release depend on several parameters, among which are the gas release flow rate ranging from low flow (e.g. flange leaks or corrosion related leaks) to high flow (e.g. pipeline full bore rupture due to third party damage) (Biezma et al.,

2020; Zhang and Weng, 2020), the release orientation, the hole diameter, the pipeline burial depth, and the ground properties (such as texture, water content, compaction layers, porosity, density). Depending on the parameters listed above, three underground gas flow regimes can be distinguished (Fig. 1): *migration*, *uplift* and *crater formation*. The migration regime is a simple diffusion of the gas in the soil with no visible modification of the morphology of the ground surface. The uplift regime is characterized by the fluidization of the soil that leads to an uplift at the ground surface, which on its extreme limits can be either low or strong. Low uplifts are accompanied with the generation of cracks in the soil, whereas the strong uplifts may lead to the formation of a crater. The crater formation regime is characterized by the complete removal of the soil above the release point so that gas is released as a free jet (Bonnaud et al., 2018; Houssin-Agbomson et al., 2018).

Several modelling (analytical and numerical) and experimental studies have been conducted on gas leakage from buried pipelines, as demonstrated in the State of the art in Section 2. However, none of the developed models tackle all the regimes simultaneously.

The analytical work is limited to studying low flow rates (diffusion) (Wakoh and Hirano, 1991; Hibi et al., 2009; Okamoto and Gomi, 2011;

* Corresponding author. Department of Chemical Engineering and Mary Kay O'Connor Process Safety Center Qatar, Texas A&M University at Qatar, Doha, Qatar.
E-mail address: k.kakosimos@qatar.tamu.edu (K.E. Kakosimos).

Okamoto et al., 2014; Parvini and Gharagouzlou, 2015) and there are empirical models produced to characterize the crater formation (Leis et al., 2002; Acton et al., 2010; Silva et al., 2016; Amaya-Gomez et al., 2018).

The computational based work has been promising and many aspects were handled; however, none of the mentioned models assessed the whole range of flow rates covering all regimes. Also, even when the soil was included, it was modelled as a porous medium; meaning that the soil representation did not reflect the real behavior expected with varying soil volume fraction along the flow to capture the regime (Wilkening and Baraldi, 2007; Ebrahimi-Moghadam et al., 2016, 2018; Deng et al., 2018; Bezaatpour et al., 2020; Cho et al., 2020; Liu et al., 2021).

Early experimental work was produced to study all regimes individually, diffusion (Hibi et al., 2009; Okamoto and Gomi, 2011; Okamoto et al., 2014; Yan et al., 2015), fluidization (Alsaydalani and Clayton, 2014), and crater formation (Acton et al., 2000; Lowesmith and Hankinson, 2013; Lutostansky et al., 2013; Cleaver and Halford, 2015; Zhou et al., 2021). The focus of these studies was to evaluate properties and expressions out of the study rather than describing the regime itself. Recent experimental work was produced to cover all the regimes by varying input parameters and visualizing the resulting regime (Bonnaud et al., 2018; Houssin-Agbomson et al., 2018). Similar studies were performed to delineate the expected regimes in a spout-fluid bed, however using characteristic velocities (Link et al., 2005, 2008; Zhang and Tang, 2006; Sutkar et al., 2013; Zhao et al., 2021). While the outcome of these studies is beneficial, they are specific to the conditions in which the experiments were carried and the correlations are not directly applicable to the risk assessment setting.

Hence, this work presents a three-dimensional computational model, instead of an expensive experimental campaign, that captures qualitatively a wide spectrum of underground gas releases and performs a boundaries delineation between the various regimes. The model's predictions aim to improve an earlier nomograph based on experimental data. This nomograph is a rapid and cost-effective screening tool to extract the regime resulting from a given release scenario (of a release force and pipeline burial depth), a key input to consequence analysis. The data of the graph is the outcome of a sensitivity analysis to study the effect of input parameters (inlet pressure, pipeline burial depth, release orientation) on the regime. The developed model adopts the Eulerian-Eulerian approach for multiphase characterization, and the kinetic theory of granular flow (KTGF) for ground representation. The optimum granular viscosity and turbulence models were selected as to validate the expected regimes from the experimental work of Houssin-Agbomson et al. (2018). As the validation was performed against qualitative data, a mechanistic approach was developed to extract the regimes with the aid of the transient spatially averaged soil volume fraction.

2. State of the art

The literature has meticulously discussed the gas diffusion

phenomenon in soil from an underground gas leak assuming the soil as a porous media i.e. utilizing Darcy's law. Wakoh and Hirano (1991) developed and validated an analytical solution of the convection-diffusion equation to estimate the transient concentration distribution, which accounted for dilute gases away from the hole, a deficiency in previous reported models. Okamoto and Gomi (2011) and Okamoto et al. (2014) used the same basis as Wakoh and Hirano (1991) in the derivation of another analytical model, but instead combined Darcy's law and Fick's law, and introduced an effective diffusion for gas (methane and propane, and hydrogen, respectively) in porous media. They also performed full scale experiments of gas leakage through a multilayer back filled pit representing a real underground gas pipeline network in order to validate their mathematical model. Hibi et al. (2009) used the dusty gas model (DGM) to represent the diffusive molar flux instead of Fick's law, as the latter is only applicable for a binary system and does not take into account the Knudsen diffusion in porous flows. The study performed experiments in a column filled with soil to validate the applicability of the model for binary and ternary systems. The work also tested Blanc's law, a simplification of the DGM in the case of a dilute tracer gas, to compare between the three models (DGM, Blanc's law, and Fick's law). Parvini and Gharagouzlou (2015) combined an enhanced porous media model (similar to Okamoto and Gomi, 2011; Okamoto et al., 2014) with a dispersion model. The enhancements included the effect of evaporation and accounted for the saturation of pores with fluid (not dry soil as the previous studies).

There has been limited research performed on the fluidization of granular beds subject to a single orifice type fluid discharge, which has been reviewed and analyzed recently by Alsaydalani and Clayton (2014). At low flow rates, for high solid volume fraction (35%–50%), the particles of the bed can affect the flow by partially sealing the orifice (Massimilla et al., 1963). Higher flow rates will cause fluidization that is first induced near the orifice, as granular soil moves away, and then in the upper layers. At this stage, Darcy's law can no longer express the complexity of the flow (Niven, 2002), and Ergun equation can be used to estimate the pressure at which fluidization occurs. Once fluidization starts, a restricted fluidization zone is created, surrounded by grains that remain fixed or move slowly. With a higher flow, the fluidized zone enlarges in the direction of the jet near the orifice but then deviates in the layers above. Finally, the fluidized zone attains the surface of the bed and becomes visible. Alsaydalani and Clayton (2014) found that the onset of fluidization is affected by the flow rate, properties of the granular material (particle size, sphericity, permeability), and bed height.

To describe the crater regime, empirical models were developed to evaluate the crater dimensions. The Gasunie model assessed the crater size using the pipeline diameter, burial depth, and a qualitative description of the soil as inputs (Leis et al., 2002). The Battelle model was enhanced through additionally incorporating the pipeline's operating pressure, specific heat ratio of the gas, and soil and gas densities (Leis et al., 2002). However, the soil classification incorporated in some

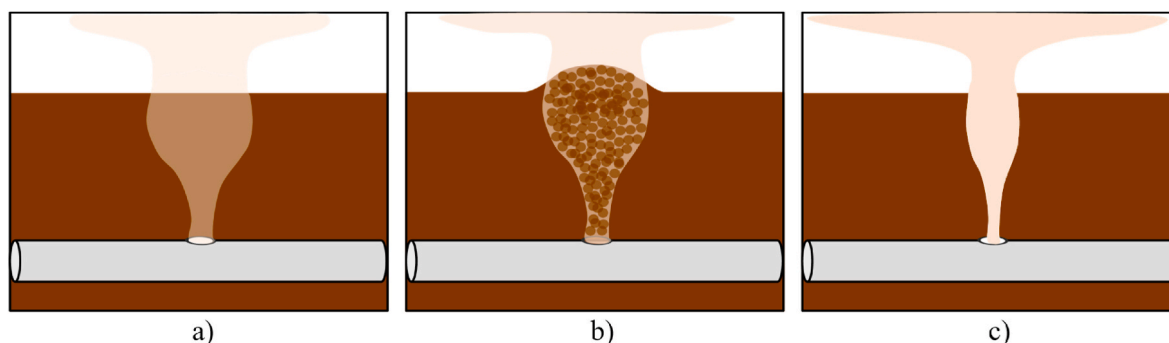


Fig. 1. The different possible underground gas flow regimes: a) migration, b) uplift and c) crater formation.

calculations was qualitative, a common gap in both Gasunie and Battelle models. Advantica model provided guidelines on the minimum separation distances between underground parallel pipelines (Acton et al., 2010). These distances were used to generate formulas for the crater width determination through linear regression, based on the pipeline pressure and diameter, and the soil type (Silva et al., 2016). The Accident-based model was established as a novel correlation based on real accidents relating the crater width, pipeline diameter, operating pressure, depth of cover, specific heat ratio of the gas, and density of the soil (Silva et al., 2016). Following the same strategy, crater dimensions were the basis for assessing the separation distance between underground pipelines for Amaya-Gomez et al. (2018) who created a more accurate probabilistic-based model for the estimation of the crater width and depth. Experimental work was conducted as well to characterize the crater regime, where the focus was on the dispersion (fire characteristics like flame height, thermal radiation, overpressure) (Lowesmith and Hankinson, 2013; Cleaver and Halford, 2015; Zhou et al., 2021) with sometimes measurements of the crater size (Acton et al., 2000; Lutos-tansky et al., 2013). The preceding work is limited to the characterization of the crater regime and the majority of the resulting contribution is empirical correlations with limited applicability of use.

Experimental work is critical to the understanding of the phenomena and the effect of the different parameters. For example, Yan et al. (2015) conducted full scale experiments to test the effect of the leaking flow rate and release orientation on the spatial and temporal concentration distribution of methane diffusing in soil from an underground pipe. Nevertheless, to the best of the authors' knowledge, none of the aforementioned models and experiments tackle all regimes simultaneously. Recently, the underground gas flow regimes were studied along a wide range of inlet pressure and other affecting parameters (Bonnaud et al., 2018; Houssin-Agbomson et al., 2018). The project 'CRATER' (2013-INNERIS), a Joint Industry Program (JIP), investigated the effect of the inlet gas pressure, gas nature, release orientation and soil nature on the regime through a series of nearly real scale experiments. The continuation project "GRTgaz" generated 101 buried pipeline releases at laboratory scale (Bonnaud et al., 2018) to study the effect of the inlet gas pressure, leak diameter, pipeline burial depth, soil type and water content. By gathering the data obtained from both studies, an empirical model was presented to predict the regime of a leak from a buried pipeline through graphs relating the regime, input release force and pipeline burial depth (Bonnaud et al., 2018). The results obtained from such studies are specific to the conditions in which the experiments were carried. This means that similar studies need to be repeated for varying conditions, and this cannot be afforded prior to each installation due to the significant time and resources required.

The experiments presented an innovative step to the field by studying the whole range of pressure from diffusion to crater formation, an essential limitation in literature. However, developing a computational model with the aid of a software, covering all the regimes, allows testing more scenarios with lower costs. Rather than focusing on the generation of the mathematical model, the computational tool allows focusing on the post-processing. Computational based studies generated expressions/methods for the evaluation of the leakage rate resulting from underground pipeline releases (Ebrahimi-Moghadam et al., 2016, 2018; Deng et al., 2018; Bezaatpour et al., 2020; Cho et al., 2020; Liu et al., 2021). They also developed contours for velocity, pressure, and concentration distribution to characterize the gas movement (Wilkening and Baraldi, 2007; Ebrahimi-Moghadam et al., 2016, 2018; Deng et al., 2018; Bezaatpour et al., 2020; Liu et al., 2021). A summary of the key points for computational studies is presented in Table 1. Two main limitations are associated with the available studies. The first one is the inclusion of soil only for the case of low pressure, under the assumption that the high pressure will eject the soil eventually. The other limitation is the characterization of soil as a porous medium rather than as a flowing phase. Describing the soil as a porous medium is common for the soil modelling in literature, as even the work adopting other approaches

for the fluids characterization (Eulerian-Eulerian, Volume of Fluid), still adopt the porous medium for the soil, in the case of methane releases from underwater soil (Geng et al., 2021). Other related work tackling subsea releases don't consider the soil presence, but rather just the leaking hole, and use the Eulerian-Lagrangian multiphase approach to study the discrete bubble particles (in analogy with the soil particles considered in this work) (Xinhong et al., 2018; Sun et al., 2020). The main explanation for these adoptions is the fact that the Eulerian models reflect better the real behavior, however, they make the computation considerably harder. Hence the characterization of the fluid phases as Eulerian, but the soil phase as a porous medium.

3. Computational model

This section describes the model development: the physical and computational domains, mathematical model, boundary and initial conditions and numerical schemes.

3.1. Physical and computational domains

The physical domain is based on Houssin-Agbomson et al. (2018), in which the authors attempted to represent a real-scale scenario. In their experiments, Houssin-Agbomson et al. (2018) used a pipeline which is 40 cm in diameter and 3 m in length. The pipeline was buried 1 m underground in a pit with dimensions: $5.5 \text{ m} \times 2.4 \text{ m} \times 3 \text{ m}$. The physical domain of the CFD model is accordingly set as shown in Fig. 2. The lower layer (ground) has a 3D rectangular shape of dimensions $5.5 \text{ m} \times 2.4 \text{ m} \times 3 \text{ m}$, in which a pipeline of 40 cm in diameter with a hole of 12 mm in diameter, was buried at a depth of 1 m (measured from the top of the pipe). The hole was placed in the middle of the pipeline and was defined as an interface between the inside of the pipeline and the outside, allowing methane to leak to the ground layer. The upper layer (atmosphere) was defined on top of the ground, with the height of 5 m.

The computational domain encapsulated the entire physical domain. It was divided into several blocks and meshed with hexahedral elements. In the vicinity of the pipeline, the elements were tetrahedral due to the curved shape. Furthermore, the mesh was refined around the pipeline and hole to improve the solution accuracy, with the smallest elements at $3.2 \times 10^{-3} \text{ m}$, whereas the biggest ones at $5 \times 10^{-2} \text{ m}$ were situated in the atmospheric domain, away from the leak. The final mesh refinement was selected by varying the maximum cell size in the different layers, for two pipeline pressures (15 bar and 40 bar), until achieving a grid independent methane average volume fraction (at five locations). The detailed results are shown in Appendix A. Eventually, the selected grid was with the finest cell size. It had 2.3 million elements and yielded an average error of 11% for the 15 bar (3%–7% for the locations above the hole, and ~20% for the left and right edges of the domain) and around 2% for the 40 bar (with no significant variations among the different locations).

3.2. Mathematical model

A three phase Eulerian approach was adopted to model the multi-phase system of air, soil, and methane coexisting in the domain, and identified by their respective volume fractions, i.e. leading to a mass and momentum conservation equation for each phase. For the momentum equation, the Boussinesq approximation introduced the Reynold's stresses, that required an additional closure/turbulence model. Five second order turbulence models were tested: the standard k- ϵ , Reynolds Normalization Group (RNG) k- ϵ , standard k- ω , baseline (BSL) k- ω and Shear Stress Transport (SST) k- ω .

Whereas the k- ϵ is frequently used to describe high Reynolds numbers, fully turbulent flows, away from walls, the k- ω is powerful at the low Reynolds numbers, and near the walls. The RNG k- ϵ was tested for its ability to better predict separated flows than the standard k- ϵ . Likewise, the BSL and SST k- ω were tested to address any gap the

Table 1

Summary of the highlights of the different computational studies.

Author(s)	Simulator	Model	Gas released	Soil modelling	Turbulence model	Key deliverables
Wilkening and Baraldi (2007)	CFD-ACE	2D and 3D Steady state and transient	Hydrogen or methane assumed as ideal	High pressure: No soil present, but rather a hole on top of the underground pipe	LES (Large Eddy Simulation)	<ul style="list-style-type: none"> • Dispersion study with/without wind through: <ul style="list-style-type: none"> ◦ Streamlines, concentration, and velocity distribution ◦ Amount of flammable mixture, thermal energy, amount of gas released
Ebrahimi-Moghadam et al. (2016)	Ansys Fluent	2D Steady state	Natural gas assumed as pure methane and ideal	Low pressure: Isotropic dry porous media	Standard k-ε	<ul style="list-style-type: none"> • Pressure and velocity distribution around the hole • Leakage volumetric flow rate expression as function of pipe diameter, pressure, and hole diameter
Ebrahimi-Moghadam et al. (2018)	Ansys Fluent	3D Steady state	Natural gas assumed as pure methane and ideal	Low pressure: Isotropic dry porous media	Standard k-ε	<ul style="list-style-type: none"> • Streamlines, pressure, velocity and Mach number distribution around the hole • Leakage volumetric flow rate expression as function of pipe diameter, pressure, and hole diameter
Deng et al. (2018)	ICEM-CFD	2D and 3D Steady state and transient	Natural gas assumed as pure methane and incompressible	<ul style="list-style-type: none"> • Low pressure: Isotropic porous media • High pressure: No soil present (use of pseudo source semi-empirical relations to imitate the soil ejection) 	Realizable k-ε	<ul style="list-style-type: none"> • Low pressure: <ul style="list-style-type: none"> ◦ Concentration distribution through the soil ◦ Dispersion study through concentration distribution at different orifice diameter and soil porosity • High pressure: <ul style="list-style-type: none"> ◦ Dispersion study through concentration distribution at different pressures, orifice diameters, and wind speed • Computation of the consequence distances used in the design of drainage systems for different parameters (pressure, orifice diameter, wind speed, and soil porosity) • Leakage flow rate as function of pipe diameter, pressure, and hole diameter. • Study of the partial saturation, anisotropy, and layer slope effects via concentration and velocity distribution of gas in soil
Bezaatpour et al. (2020)	COMSOL	3D Transient	Natural gas considered as a mixture of methane, ethane, and propane and characterized through the Soave-Redlich-Kwong equation of state and mass transfer	Low pressure: Anisotropic partially saturated multilayer porous media <ul style="list-style-type: none"> • each layer has its properties (texture, porosity, variable moisture with time, slope) • mass transfer account for thiol adsorption into soil 	Reynolds stress components and effective stress tensor considered	<ul style="list-style-type: none"> • Use of a dimensionless number relating gas surface concentrations, subsurface parameters (of gas and soil), and volumetric leakage rate to deduce the flow rate released from measured surface concentrations on spot during a regular leak survey • Leakage flow rate estimation model as function of pressure, leakage hole diameter, soil porosity and particle diameter • Concentration distribution prediction model through the soil at different times and positions from the hole for various leakage rates • Effect of pressure, hole diameter and shape, temperature, soil depth and properties on the gas diffusion via soil • Characterization of the gas dispersion in air
Cho et al. (2020)	TOUGH3/EOS7CA	3D Steady state	Methane modelled by Peng-Robinson equation	Low pressure: Porous media with the presence of water and brine as components	Not modelled	<ul style="list-style-type: none"> • Use of a dimensionless number relating gas surface concentrations, subsurface parameters (of gas and soil), and volumetric leakage rate to deduce the flow rate released from measured surface concentrations on spot during a regular leak survey • Leakage flow rate estimation model as function of pressure, leakage hole diameter, soil porosity and particle diameter • Concentration distribution prediction model through the soil at different times and positions from the hole for various leakage rates • Effect of pressure, hole diameter and shape, temperature, soil depth and properties on the gas diffusion via soil • Characterization of the gas dispersion in air
Liu et al. (2021)	Ansys Fluent	3D transient	Air or natural gas assumed as pure methane	Low pressure: Isotropic dry porous media	Standard k-ε	<ul style="list-style-type: none"> • Use of a dimensionless number relating gas surface concentrations, subsurface parameters (of gas and soil), and volumetric leakage rate to deduce the flow rate released from measured surface concentrations on spot during a regular leak survey • Leakage flow rate estimation model as function of pressure, leakage hole diameter, soil porosity and particle diameter • Concentration distribution prediction model through the soil at different times and positions from the hole for various leakage rates • Effect of pressure, hole diameter and shape, temperature, soil depth and properties on the gas diffusion via soil • Characterization of the gas dispersion in air

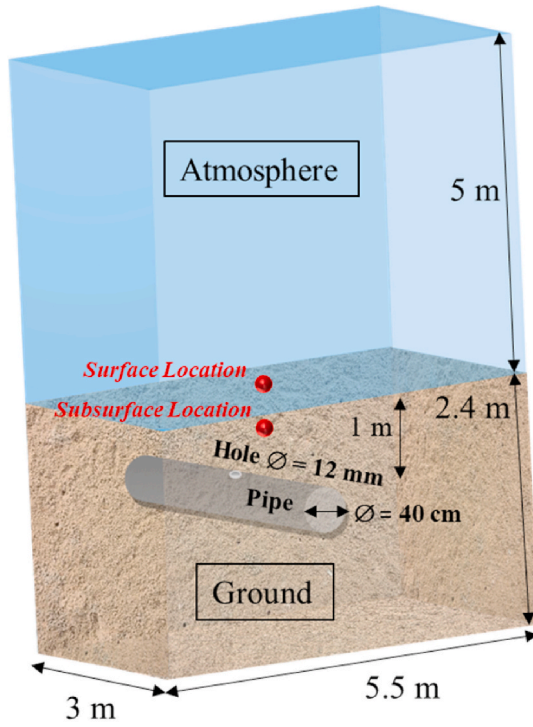


Fig. 2. The 3-dimensional domain of the geometry displaying the two layers (ground and atmosphere), the pipeline, and the hole. The dimensions and auxiliary locations are also denoted.

standard $k-\omega$ might have as per the behavior in free streams. The SST $k-\omega$ might have a superiority in describing boundary layers under adverse pressure gradients but the standard $k-\omega$ is more appropriate for compressible flows (Menter, 1994; Markatos, 2012; Argyropoulos and Markatos, 2015). Finally, the choice of the turbulence model was dictated by its ability to predict the experimental results for the range of pressures, and its computational time.

The granular solid phase (soil, represented by s) was characterized by a stress tensor in the solid phase momentum balance (Eq. (1)) which similarly required a closure model.

$$\frac{\partial}{\partial t} (\alpha_s \rho_s \vec{v}_s) + \nabla \cdot (\alpha_s \rho_s \vec{v}_s \vec{v}_s) = -\alpha_s \nabla p - \nabla p_s + \nabla \cdot \vec{\tau}_s + \alpha_s \rho_s \vec{g} + \beta (\vec{v}_g - \vec{v}_s) \quad (1)$$

Herein, this closure was provided through the kinetic theory of granular flow (KTGF) (Ding and Gidaspow, 1990). According to the KTGF, the solids stress tensor (i.e. the origin of the granular characteristics of the solid phase) is a function of the strain rate, solids pressure, and bulk and shear viscosities.

The **solids pressure** and the **viscosities** depend on the granular temperature and on the radial distribution function. The **radial distribution function** is a correction term that modifies the probability of collision when close to reaching the packing limit. The solids pressure and the radial distribution function were both characterized by Lun et al. (1984). The **granular temperature**, in analogy with the thermodynamic temperature for gases, is a measure of the energy resulting from the fluctuating velocity of the particles. The granular temperature is described with the differential form of the solids fluctuating energy conservation equation. Alternatively, in this work, an algebraic formulation was employed to simplify the computational time, neglecting diffusion and convection in the transport equation, with the rate of energy dissipation due to particles collisions represented by Lun et al. (1984) and the transfer rate of kinetic energy due to random collisions between the gas and solid phases described by Gidaspow et al. (1992).

The **bulk viscosity** accounts for the resistance of the granular particles to compression and expansion, and it was described by Lun et al. (1984). The **shear viscosity** accounts for the tangential forces, which are prescribed by the following forms of granular dissipation, according to the KTGF (Darteville, 2003):

- In a dilute region of the flow, the particles randomly fluctuate and the viscous dissipation is kinetic.
- In a more concentrated region, some particles start colliding and the viscous dissipation is now kinetic and collisional.
- At very high concentrations, when the particles reach the maximum solid volume fraction, the particles are in enduring contact and the sliding becomes frictional.

Thus, the shear viscosity is comprised of the **granular (or kinetic) viscosity**, **collisional viscosity**, and **frictional viscosity**. The **granular viscosity** accounts for the kinetic fluctuations and is frequently described by the Gidaspow and Syamlal-O'Brien models (Gidaspow et al., 1992; Syamlal et al., 1993), which were both explored. The particles are modelled as inelastic in the Syamlal-O'Brien model and as elastic in the Gidaspow model. Noteworthy, the energy dissipation due to the inelastic collisions causes higher pressure drop across a packed bed, and consequently, larger bubbles and aggressive movement are produced by the higher force of the flow (Hilmee et al., 2013). The **collisional viscosity** accounts for the collisions of the particles, and was described by the expression of Gidaspow et al. (1992). The **frictional viscosity** accounts for the viscous-plastic transition at maximum solid volume fraction, and was modelled with the expression of Schaeffer (1987). The drag coefficient between the different phases was described through the correlation of Schiller and Naumann (1935).

The detailed multiphase mathematical model, including the conservation laws and the constitutive equations, is presented in Appendix B.

Specifically, the kind of sand used in the experimental work of Houssin-Agbomson et al. (2018) is SP-SM according to the USCS (Unified Soil Classification System Soil and Rock (2017)). This classification gives general guidelines about ranges of density, water content and particle diameter. For the sand, the range of density is 1600–2000 kg/m³. Hence, a packing limit (i.e. the solid volume fraction at inter-particle contact) of around 60% was estimated; however, the guidelines yield a wider range. Therefore, the sand was modelled with a density of 1800 kg/m³ and a packing limit of 63% corresponding to the spherical packing limit and close to the estimated one. According to the same guidelines, around 40% of the SP-SM particles' diameter ranges between 0.075 mm and 4.75 mm while 12% can be lower than that. Therefore, a constant particle diameter of 0.1 mm was selected, which was the maximum one allowing for the numerical solver to converge. The main properties of the different phases used throughout the work are summarized in Table 2.

Table 2
Main properties of the different phases.

Component (Phase)	Property	Value
Air	Density (kg/m ³)	1.225
	Viscosity (Pa·s)	1.7894 × 10 ⁻⁵
Methane	Density (kg/m ³)	0.6679
	Viscosity (Pa·s)	1.087 × 10 ⁻⁵
Soil	Density (kg/m ³)	1800
	Particle diameter (mm)	0.1
	Packing limit (–)	0.63
	Restitution coefficient of particle-particle collisions (–)	0.9
	Angle of internal friction (degree)	30.00007

3.3. Boundary and initial conditions

In this study, the boundary conditions were defined in accordance with the experimental work (Houssin-Agbomson et al., 2018). They included the following: pressure inlet, pressure outlet and wall boundary conditions. The intersection boundary of the fluid in the pipeline and the soil in the ground at the hole was defined as an interface. The boundary type associated with the selected boundaries are summarized in Table 3.

The volume fraction in the computational domain was initialized with 100% air in the atmosphere, 100% methane in the pipeline, and 63% soil in the ground representing the packing limit (with the balance air).

3.4. Numerical schemes

The mathematical model was solved using an unsteady pressure-based solver (ANSYS Fluent version 18.2) with the SIMPLE pressure-velocity coupling. The First Order Upwind scheme was selected for all the spatial discretization. The transient formulation was solved using the First Order Implicit scheme. The under-relaxation factors were varied accordingly to achieve convergence of the results, reaching values as low as 0.1 for the turbulence and pressure. A time stepping method was chosen with a truncation error tolerance and a time step size of 0.001 and 0.001 s, respectively. All simulations were executed using 16 or 24 CPUs at the high-performance computing (RAAD2: Cray® XC40-AC with 4128 Intel Xeon E5-2690 V3 CPUs across 172 Nodes) facilities at Texas A&M University at Qatar.

The use of the first order schemes is usual for studies on related physical models e.g. large spout-fluid beds at high pressure and temperature (Zhong et al., 2007), prismatic fluidized beds (Gryczka et al., 2009), bubbling fluidized beds (Hilmee et al., 2013), the well-cited comparison of Euler-Euler with Euler-Lagrange models for spouted beds (Almohammed et al., 2014), and most recently study of a circulating fluidized bed riser (Upadhyay et al., 2020). One of the reliable evidences that the numerical scheme does not probably affect the regime of the flow has been presented by Hosseini et al. (2013) who inter-compared the numerical schemes for the granular flow in spouted beds (e.g. Fig. 8 on the voidage in the spout zone), although they do affect the prediction of fountain height and particle velocity.

4. Mechanistic approach for the regime identification

As it was mentioned in Section 2, there is a lack of quantitative underground gas release experiments that cover all regimes, apart from the qualitative work of Houssin-Agbomson et al. (2018) and Bonnaud et al. (2018). Therefore, a mechanistic approach was devised to extract the regime using results from the numerical simulation; in particular, the transient spatially averaged soil volume fraction (VF) at one or more auxiliary locations (surface and/or subsurface, as shown in Fig. 2). Most of the times, a single location should be sufficient to extract the regime, however, the additional location could be used for verification. According to the mechanistic approach:

At the surface location, the VF remains low (close to zero) over time for the migration case (Fig. 3a) as no soil gets displaced to that region. Beyond migration, a higher gas release force displaces the soil, and the

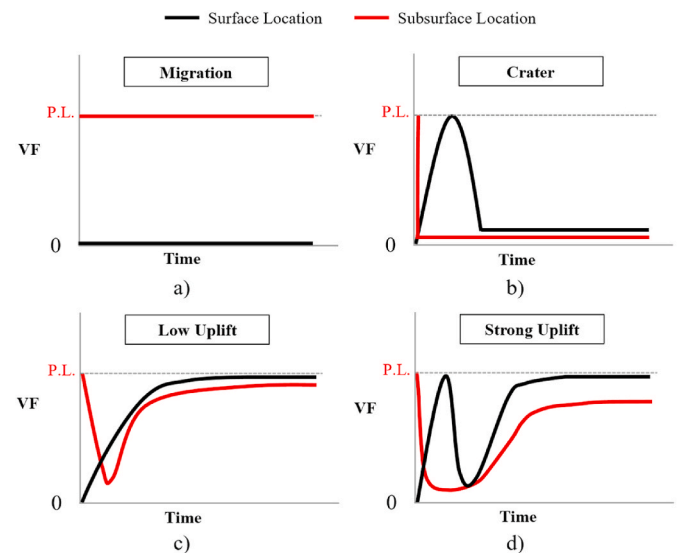


Fig. 3. The VF at the surface location and the subsurface location to extract each of the four regimes: a) migration, b) crater, c) low uplift and d) strong uplift, according to the mechanistic approach. P.L. stands for Packing Limit.

VF increases gradually to approach the packing limit. Hence, for the low uplift case (Fig. 3c), the VF stabilizes at the packing limit, as the ground slightly rises. In contrast, for the extreme case of a crater (Fig. 3b), this increase is followed by a drop to a significantly smaller value as the gas displaces the uplifted soil. For the intermediate case of a strong uplift (Fig. 3d), this drop is followed by a rise again to the packing limit, as this regime resembles intense bubbling by oscillating between an uplift and a crater.

A similar analogy is followed at the subsurface location, where the VF remains at the packing limit for the migration case (Fig. 3a), as the gas diffuses through the pores without displacing the soil. Beyond migration, the VF drops to a low value (depending on the regime), indicating the presence of cracks and/or soil displacement. For the extreme case of a crater (Fig. 3b), the soil is completely displaced and so the VF stabilizes at this low value. For the low uplift case (Fig. 3c), the VF restores back to a value equal or slightly less than the packing limit. Similarly, for the strong uplift (Fig. 3d), the VF gradually goes back to a value, between the ones achieved during a low uplift (~packing limit) and a crater (~0), however, with a wider slope (i.e. at a slower restoration rate).

This mechanistic approach reflects an ideal interpretation of the flow behavior and the VF for each regime. However, a 5% VF for example instead of strictly 0% may still represent a significant soil displacement and crater formation. This was necessary as the Eulerian-Eulerian multiphase approach approximates the solid behavior (soil considered as a fluid) that prohibits capturing the real patterns. Accordingly, the suggested values and slopes can be considered only indicative, and a certain tolerance is acceptable as long as the general behavior of the regime is present. It is noteworthy to mention that the range of regimes from a migration to a crater formation encapsulates numerous observations and is not limited to the strict regime itself.

5. Qualitative validation

The qualitative validation was performed in sequence at three pressures while varying the turbulence model and the granular viscosity model (Table 4), in order to identify the optimum configuration by elimination. Note that all initial turbulence models testing was performed with the Gidaspow granular viscosity model.

Table 3

Boundary conditions adopted in this study.

Boundary location	Boundary type
Inlet and outlet of the pipeline	Inlet pressure (corresponding to the trial)
Lateral surface of the pipeline	Wall
Hole	Interface (on ground and on pipe)
Ground surface	Interface (on ground and on atmosphere)
Boundary surfaces of the soil	Walls
Boundary surfaces of the atmosphere	Pressure outlet (atmospheric)

Table 4

The parameters and property varied to perform the model validation.

Parameter/Property	Trials
Pressure in bar (expected regime)	1 (migration), 15 (low uplift), 66 (crater)
Turbulence model	Standard k- ϵ , RNG k- ϵ , Standard k- ω , BSL k- ω , SST k- ω
Granular viscosity model	Gidaspow, Syamlal-O'Brien

5.1. Turbulence model

According to the mechanistic approach in Section 4, at the pressure of 1 bar (Fig. 4a and b), both k- ϵ models predicted a slight uplift with cracks in the soil. The standard k- ω model clearly predicted a migration, as expected, at both subsurface (VF maintained at the packing limit) and surface locations (VF stayed 0). The remaining k- ω models predicted an in between condition. As a result, both k- ϵ models were eliminated from further evaluation. This is expected as the k- ϵ model is usually used for fully turbulent cases at high pressures (Menter, 1994; Soe and Khaing, 2017). Nevertheless, the standard k- ϵ was included in the next pressure test for comparison and reference.

The BSL k- ω and SST k- ω models yielded closer results to the standard k- ω model rather than the standard k- ω model at 15 bar (Fig. 4c). While the BSL k- ω , SST k- ω and standard k- ϵ predicted a strong uplift (approaching a crater) as the VF converged to a low value (20%) after the initial variation, the standard k- ω converged back to a high value (close to the packing limit) after the initial decrease indicating minor cracks and a low uplift regime. Hence, the standard k- ω was the closest in estimating the experimental observation of low uplift and the other models could be eliminated. However, the SST k- ω model was included in the next pressure test for comparison, and because the SST k- ω model is among the most advanced models, enhanced to better describe the free jet behavior (Menter, 1994), which is expected when the crater forms at high pressures.

Indeed, at the pressure of 66 bar (Fig. 4d), the SST k- ω predicted a crater formation (VF approached zero at the subsurface location), which is the expected regime. On the other hand, the standard k- ω model predicted at most a strong uplift.

Although the standard k- ω model under-estimated the expected regime at high pressures, as it has some weaknesses when it comes to

free streams (Menter, 1994), it allowed the visualization of regimes that were not achievable with other models, and it covered a major part of the pressure range as shown in Table 5. Accordingly, to proceed, this model was selected. However, as the validation isn't complete yet, the viscosity model, investigated next, could potentially solve the problem at high pressures.

5.2. Granular viscosity

After fixing the standard k- ω turbulence model, the granular viscosity models were tested at the different pressures as presented in Table 4. At the pressures of 1 bar and 15 bar, as shown in Fig. 5a and b, respectively, both granular viscosity models predicted identical results, validating the expected regimes of migration and low uplift, respectively. This may be due to the fact that the impact of collisions at low pressure is negligible as the soil particles are mostly static. Consequently, both granular viscosity models were tested at the next pressure of 66 bar.

At the pressure of 66 bar (Fig. 5c), Syamlal-O'Brien model predicted a crater formation (VF remained low after the initial drop), which is the expected regime. This result was in contrast to what was predicted by the Gidaspow model (uplift), as discussed previously in the turbulence model testing (Fig. 4d). This can be associated to the different approaches of the granular viscosity models in the description of the collisions between the soil particles. The energy dissipation from inelastic collisions, as described by Syamlal-O'Brien model, causes higher pressure drop, which in turn allows for the displacement of the soil and

Table 5

The regimes anticipated from the different turbulence models at the different pressures. The colored box refers to the expected regime. The vertical alignment of the symbols indicates the regime.

Pressure (bar)	Regime			
	Migration	Low Uplift	Strong Uplift	Crater
1	●	■	▲	
15		●	■	▲
66			●	■

▲: Standard k- ϵ ●: RNG k- ϵ ■: BSL k- ω ◆: SST k- ω ●: Standard k- ω

▲: Standard k- ϵ ●: RNG k- ϵ ■: BSL k- ω ◆: SST k- ω ●: Standard k- ω

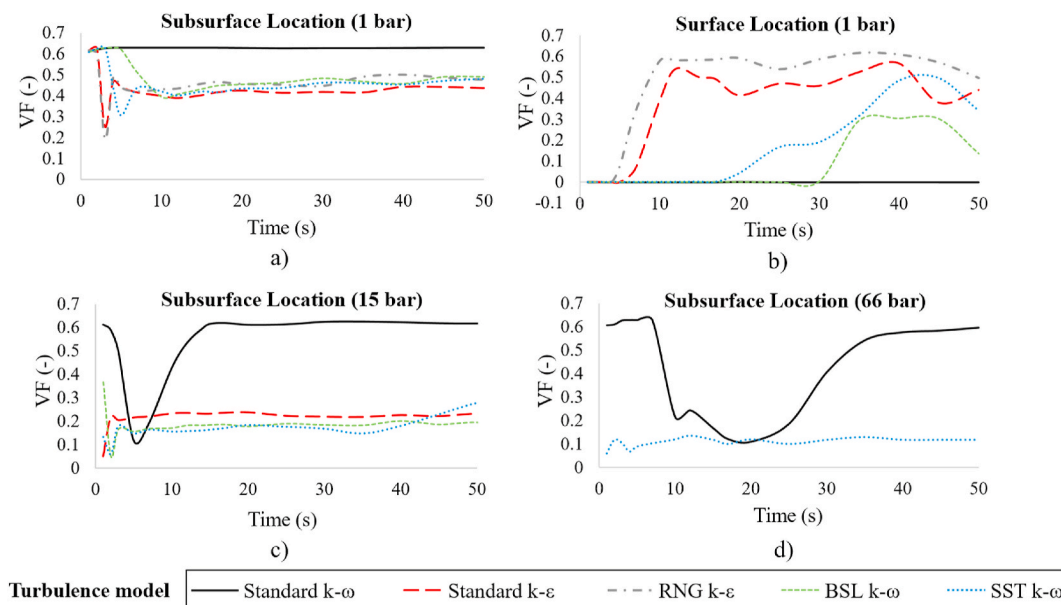


Fig. 4. Time-series of VF for the different turbulence models at the subsurface location and the surface location at: a) and b) 1 bar (migration), and at the subsurface location at: c) 15 bar (uplift) and d) 66 bar (crater).

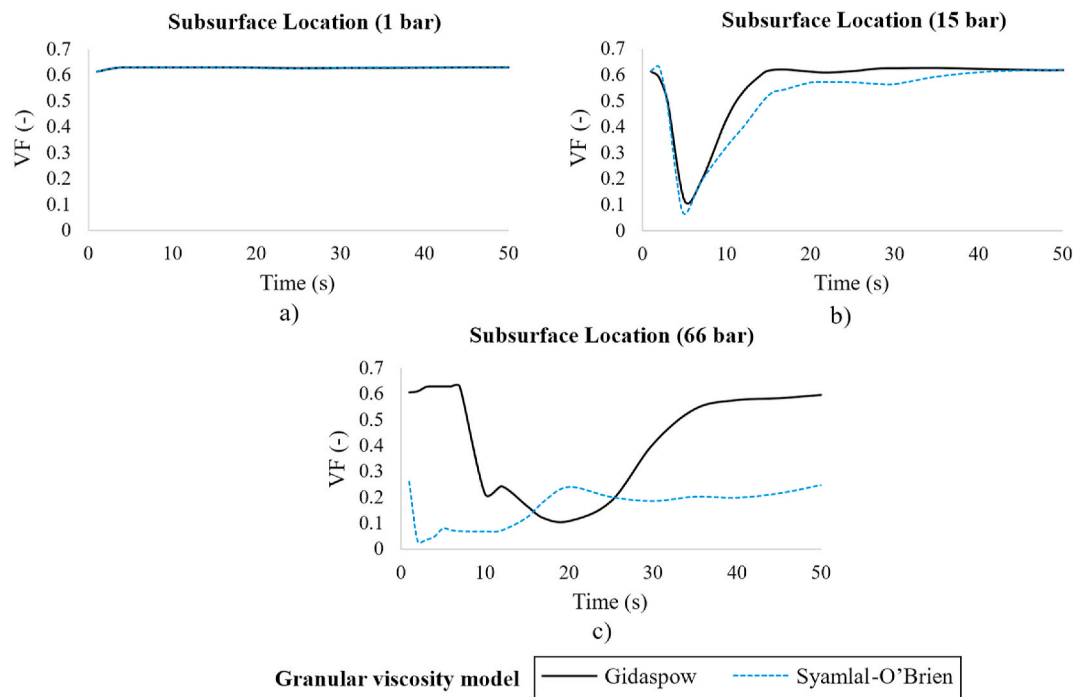


Fig. 5. Time-series of VF for the different granular viscosity models at the subsurface location at: a) 1 bar (migration), b) 15 bar (uplift) and c) 66 bar (crater).

generates crater at high pressures (Hilmee et al., 2013), whereas the elasticity of the soil particles assumed in Gidaspow model results in an under-estimation of that regime.

Hence, the Syamlal-O'Brien granular viscosity model improved the standard $k-\omega$ turbulence model. Their combination successfully predicted the regimes at all pressures, and consequently, they were selected to proceed with the sensitivity analysis.

The regime identification and the model configuration were deduced from the above plots of the transient spatially averaged soil volume fraction after analysis due to the shortcomings of the Eulerian-Eulerian model to fully characterize the soil. A clear illustration of this fact is the crater case in Fig. 5c. The jet behavior expected in the case of crater formation (66 bar) could not be fully represented as the soil approximation to a fluid inaccurately allows the soil to fall back in the crater. This is demonstrated by the soil volume fraction that doesn't remain zero, as it ideally should be, but settles to an average of less than 15%. Despite its shortcomings, this model proved capable of describing the general behavior sufficient to extract the regime.

While this study performed a qualitative validation and focused on the regimes, the quantitative data extracted from the model can aid in the characterization of the release. For example, the local Mach number at the hole conditions (i.e., velocity, diameter) suggested that the flow goes from subsonic to sonic across the wide range of the pressures examined and the identified regimes, from migration (with Mach ~ 0.2 – 1.1), to uplift (Mach ~ 2 – 4.6) and up to the crater formation (Mach ~ 5.8 – 6.4). This is in accordance with earlier literature which reported subsonic flows for the migration regime, and sonic flows beyond that (Ebrahimi-Moghadam et al., 2018). Other derived quantities like the local Reynolds number followed similar patterns ranging $\sim 4.7 \times 10^4$ – 2.7×10^5 for migration, $\sim 5 \times 10^5$ – 1.2×10^6 for uplift and $\sim 1.5 \times 10^6$ – 1.6×10^6 for crater formation. The release flow rate was also closely related to the regime with values ranging $\sim 7.2 \times 10^{-3} \text{ m}^3/\text{s}$ – $4.2 \times 10^{-2} \text{ m}^3/\text{s}$ for diffusion, $\sim 7.6 \times 10^{-2} \text{ m}^3/\text{s}$ – $1.8 \times 10^{-1} \text{ m}^3/\text{s}$ for uplift, and $\sim 2.2 \times 10^{-1} \text{ m}^3/\text{s}$ – $2.5 \times 10^{-1} \text{ m}^3/\text{s}$ for crater formation. In our future work, we will aim to correlate directly the Reynolds and Mach numbers with the regime and flow rate, instead of the simpler mechanistic approach.

6. Results

Three parameters were selected to conduct a sensitivity analysis according to the literature and typical risk assessment studies: the inlet pressure, pipeline burial depth (or height), and release orientation. Also, this data was incorporated into the nomograph generation.

The inlet pressure was varied (0.35 bar–75 bar) while fixing the pipeline burial depth (1 m) and the release orientation (upwards). The time-series of VF at the surface location and the subsurface location are displayed in Fig. 6. Pressures below 6 bar resulted in migration, as the soil was not displaced either at the surface or at the subsurface locations. At the pressure of 6 bar, a very slight movement was detected but it did not reach the level of low uplift. In addition, the VF time-series corresponding to 6 bar was closer to those of the lower pressures rather than to the one of 15 bar, which resulted in a low uplift. Accordingly, 6 bar can be considered as a transition pressure between the migration and low uplift regimes for the defined geometry and type of soil.

At the pressures of 15 bar and 27 bar, the soil was displaced to the surface location, and cracks were revealed at the subsurface location (VF converged close to 63%). The same occurred to the following pressures up to 50 bar, with slight variations. These pressures caused more intense forces and openings, as represented by the sharper gradients of the VF. At the higher pressures, the VF eventually stabilized at low values (less than 20%) at both locations, reflecting an expelled soil i.e. crater formation.

It can be seen, especially for the subsurface location, that the different regimes can be distinguished according to their trendlines. Hence, the different sets of pressures can be attributed to the different regimes.

Three pipeline burial depths were tested (30 cm, 60 cm, and 100 cm) at three different pressures (6 bar, 15 bar, and 50 bar), and an upward release orientation. These specific depths were selected to fill some of the gap in the nomograph discussed later in this section, as Bonnaud et al. (2018) tested only low depths (up to 17 cm) and Houssin-Agbomson et al. (2018) tested only the depth of 100 cm.

At the pressure of 6 bar and a depth of 100 cm, the resulting regime was a migration, whereas for the depths of 60 cm and 30 cm, the model predicted a low uplift and a strong uplift, respectively. At the next

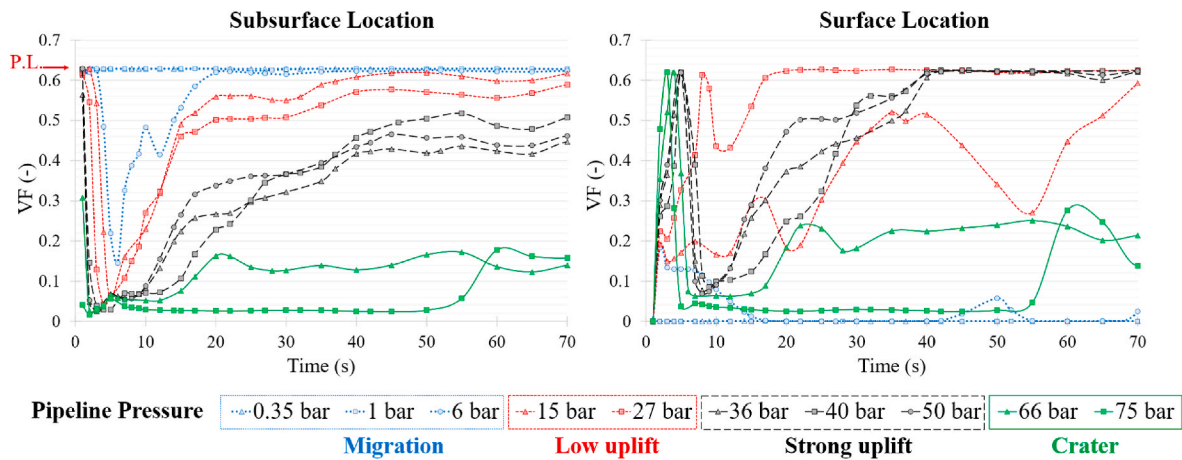


Fig. 6. Time-series of VF at the subsurface location and the surface location for the different studied pressures, categorized according to the regime. P.L. stands for Packing Limit.

pressure of 15 bar and a depth of 100 cm, the resulting regime was a low uplift (Fig. 7a), whereas a strong uplift was predicted for 60 cm (Fig. 7b), and a crater for 30 cm (Fig. 7c). Hence, the lower the pipeline burial depth, the more probable is for a crater to be formed for the same release conditions (inlet pressure, ground properties, burial depth, release orientation).

A higher inlet pressure and a lower pipeline burial depth favor the formation of a crater. A higher gas pressure (assumed to be the same along the pipeline and at the hole in this work and in the experiment of Houssin-Agbomson et al. (2018)) leads to a higher force exerted by the gas which resists the weight of the soil bed. The higher force will provoke a higher advection next to the hole due to a larger pressure drop, eventually causing more aggressive soil displacement. Moreover, soil displacement is more likely for a lower burial depth, as the soil resistance to the upward movement is lower. Hence, it is easier for the gas flow to lift the soil above the hole.

All the analysis herein was performed at an upward release orientation, which is expected to trigger the worst consequences. However, the release orientation has been reported to significantly affect the methane surface concentration distribution (Vianello and Maschio, 2014; Yan et al., 2015; Houssin-Agbomson et al., 2018), and even the regime (Houssin-Agbomson et al., 2018). To verify its effect, four different release orientations were tested: vertical (upward and downward) and horizontal (left and right), at a pressure corresponding to a crater formation at the upward release orientation. Eventually, none of the orientations, but the upward, triggered a crater; as they produced an

uplift. This observation agrees with the experimental one. Specifically, Houssin-Agbomson et al. (2018) deduced that, for sandy soil, no crater is expected unless the release orientation is upward – at least for pressures up to 75 bar and a hole of 12 mm in diameter. Further studies should be conducted to capture the effect of the release orientation on the regime.

Bonnaud et al. (2018) combined their experimental data with that of Houssin-Agbomson et al. (2018) to develop a zoning graph – nomograph – for the identification of the regime resulting from underground gas releases. This nomograph starts as a plot of the pipeline burial depth (height) versus the force of the released gas (ratio of the inlet pressure to the cross-sectional area of the hole), and includes four different zones, one for each of the regimes. To identify each regime, Bonnaud et al. (2018) assigned a dimensionless and qualitative coefficient according to the regime, ranging between 0% and 100%, with 0% representing migration and 100% an intense crater. In addition, they defined in between levels for all the regimes, see Table 6. Taking the example of the migration regime, a coefficient of zero implies a gas migration with no cracks at all, whereas a coefficient of 17% implies a migration with small cracks.

The significance of such nomograph lies in the fact that it generalizes the results and serves as a tool to extract the regime. A computational model allows the analysis to be conducted safely, while saving time, effort, and costs. However, a numerical case might still require a significant time to generate results due to the complexity of the established model (transient, wide range of pressure, Eulerian-Eulerian multiphase, and turbulent scenario). For practicality, this study emphasizes on the importance of a nomograph that would enable safety engineers to readily extract the regime, a crucial input for risk assessment. Therefore, the model's results were generated to prove its applicability and ability to improve the resolution of the earlier developed nomograph.

The main challenge of this nomograph is the gap between the tested depths, as Bonnaud et al. (2018) tested only low depths (up to 17 cm) and Houssin-Agbomson et al. (2018) tested only the depth of 100 cm. Moreover, the transition to crater formation was well defined but the transition between migration and uplift was not, as it is more difficult to capture it. Accordingly, the sensitivity analysis of the computational model was used to fill in the depths gap and narrow down the delineation of the boundaries between the regimes, as displayed in Fig. 8. For example, in the original nomograph, the transition from migration to uplift (at a 100 cm depth), was identified between ~6 N and 90 N, but the computational model narrowed this down to between ~67 N and 90 N.

While the introduction of a universal computational model is promising, there are several critical points that require further investigation such as the regime identification and ground representation. For

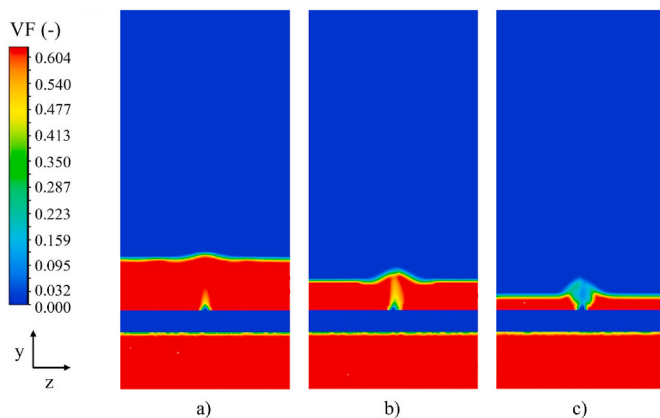


Fig. 7. Visualization of VF at a cross-sectional plane ($x = 1.5$ m, the position of the hole) for a pipeline burial depth of: a) 100 cm (low uplift), b) 60 cm (strong uplift), and c) 30 cm (crater) at the pressure of 15 bar.

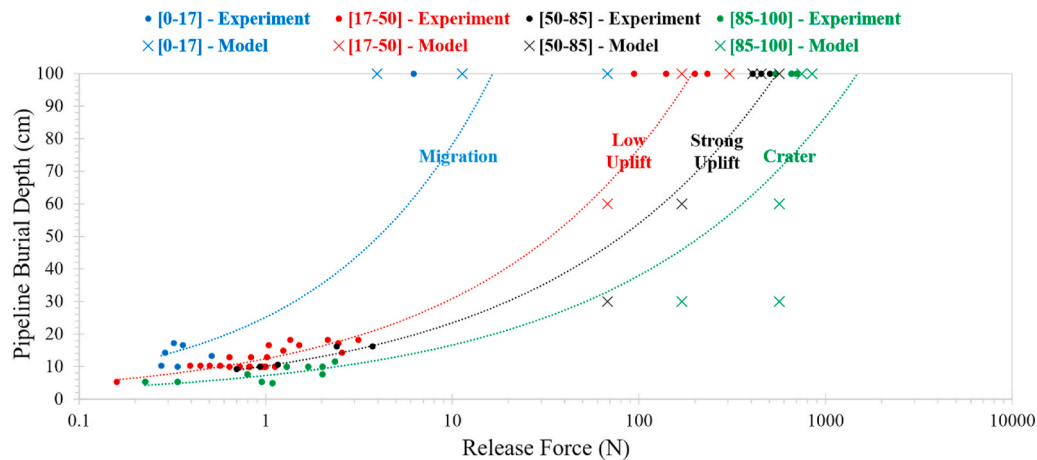


Fig. 8. Nomograph to extract the regime associated with a release scenario of a given release force and pipeline burial depth at an upward release orientation.

Table 6

The regimes expressed in terms of the qualitative coefficient.

Release outcome in sand	Coefficient (%)	Regime
Migration – Migration with small cracks	0–17	Migration
Cracks with Uplift	17–50	Low Uplift
Cracks with Uplift accompanied with a crater	50–85	Strong Uplift
Stable Crater after uplift – instantaneous Crater	85–100	Crater

instance, [Bonnaud et al. \(2018\)](#) implied that over longer release durations, the regime can scale up (from a migration to an uplift and from an uplift to a crater). Hence, it may be important to extend the duration of both the experimental and numerical observations to capture such effects. In parallel, it is important to develop a quantitative metric to monitor the transient evolution of the regime, rather than just a qualitative observation of a steady state result. In addition, the soil properties require extension to include various types of soil (sand, clay), compaction layers, and transport properties. The water content is another aspect that should be accounted for as it alters the soil cohesion and subsequently the gas flow ([Bezaatpour et al., 2020](#)). Moreover, the temperature variations should be considered because of the Joule-Thomson effect on the release and ground properties ([Wang et al., 2019](#)). Finally, as more computational and experimental data are produced, the nomograph can be expanded e.g. pipeline burial depth, release orientation.

7. Conclusions

A three-dimensional computational model was proposed for underground gas flow releases from buried pipelines spanning a wide range of flow regimes. In particular, the soil was considered a granular phase under a Eulerian-Eulerian multiphase approach. The numerical results were qualitatively validated against experimental data by means of a mechanistic approach developed to provide guidelines for regime identification. Following the developed mechanistic approach, the optimum models were selected by elimination, eventually leading to the standard $k-\omega$ turbulence model and the Syamlal-O'Brien granular viscosity model. By analysis of the numerical simulations, it was shown that a higher pipeline pressure, a lower pipeline burial depth and an upward release orientation favor the formation of a crater. The data was added to an existing empirical nomograph that allows the extraction of the regime using the pipeline burial depth and pressure (or force).

The qualitative evaluation supported the capacity of the model to identify the regimes. However, future work should adopt higher order numerical schemes to enhance the accuracy of the results. Moreover, the Eulerian-Eulerian multiphase approach was incapable of capturing the

exact behavior of the soil, like the creation and evolution of fractures, channels, and the permanent displacement. Hence, the ground modelling approach should be revisited to evaluate its performance relative to alternative representations e.g. Eulerian-Lagrangian and new viscosity models. Similarly, the validity of the modelling approach should be further verified over a wider range of parameters (e.g. extend to different soil types and characteristics, consider hole diameters aside the 12 mm breach scenario, variable particle size distribution and temperature variations).

In the future, a universal high-fidelity model can directly predict the ambient release rates driven by underground pipeline leaks. However, such a high-fidelity model will require significant computational resources and time to complete the multiple simulations required in risk analysis studies. The enhanced nomograph presented in this work assists the safety engineer with identifying the regime. Accordingly, the engineer can select between several available formulations such as the Darcy type of models for migration ([Ebrahimi-Moghadam et al., 2018](#); [Bezaatpour et al., 2020](#)) and Advantica or Accident-based model for crater formation ([Acton et al., 2010](#); [Silva et al., 2016](#)) based on the readily available information of the risk analysis e.g. pipeline pressure and hole diameter.

Credit author statement

Ola Srour: Conceptualization, Methodology, Software, Data Curation, Writing - Original Draft, Visualization; **Konstantinos E Kakosimos:** Conceptualization, Methodology, Writing - Review & Editing, Supervision, Project administration; **Luc Vechot:** Conceptualization, Funding acquisition, Writing - Review & Editing, Supervision.

Declaration of competing interest

The authors declare the following financial interests/personal relationships which may be considered as potential competing interests: Konstantinos Kakosimos reports financial support was provided by Qatar Foundation. Konstantinos Kakosimos reports financial support was provided by Texas A&M Mary Kay O'Connor Process Safety Center.

Data availability

Data will be made available on request.

Acknowledgments

This publication was made possible by the support of the Mary Kay O'Connor Process Safety Center at Qatar. The statements made herein

are solely the responsibility of the authors. The High-Performance Computing resources and services used in this work were provided by

the Research Computing group in Texas A&M University at Qatar. Open Access funding provided by the Qatar National Library.

Appendices A & B. Supplementary data

Supplementary data to this article can be found online at <https://doi.org/10.1016/j.jngse.2022.104832>.

Nomenclature

α	volume fraction, dimensionless
ρ	density, kg/m ³
\vec{v}	velocity vector, m/s
p	pressure, Pa
$\bar{\tau}$	stress-strain tensor, Pa
g	acceleration of gravity, m/s ²
β	interphase momentum exchange coefficient between the phases, kg/m ³ s
μ	viscosity, kg/m s
λ	bulk viscosity, kg/m s
d	particle diameter, m
θ_s	granular temperature, m ² /s ²
e_{ss}	restitution coefficient, dimensionless
g_0	radial distribution function, dimensionless
$\alpha_{s,max}$	maximum solid volume fraction (packing limit), dimensionless
I_{2D}	second invariant of the deviatoric stress tensor, dimensionless
φ	angle of internal friction, degree
k_{θ_s}	diffusion coefficient for the granular energy, kg/m s
γ_{θ_s}	collisional dissipation of energy, kg/m s ³
φ_{gs}	transfer rate of kinetic energy, kg/m s ³
f	drag function, dimensionless
C_D	drag coefficient, dimensionless
Re	Reynolds number, dimensionless
τ_s	particulate relaxation time, s
k	turbulent kinetic energy, m ² /s ²
ε	dissipation rate of turbulent energy, m ² /s ³
ω	dissipation per unit kinetic turbulence energy, 1/s

Subscripts

g	gas
s	solid
q	phase g or s
max	maximum

References

- Acton, M.R., Hankinson, G., Ashworth, B.P., Sanai, M., Colton, J.D., 2000. A Full Scale Experimental Study of Fires Following the Rupture of Natural Gas Transmission Pipelines. Paper presented at the 2000 3rd International Pipeline Conference.
- Acton, M.R., Jackson, N.W., Jager, E.E., 2010. Development of guidelines for parallel pipelines. Paper presented Int. Pipeline Conf.
- Almohammed, N., Alobaid, F., Breuer, M., Epple, B., 2014. A comparative study on the influence of the gas flow rate on the hydrodynamics of a gas–solid spouted fluidized bed using Euler–Euler and Euler–Lagrange/DEM models. *Powder Technol.* 264, 343–364.
- Alsaydalani, M., Clayton, C., 2014. Internal fluidization in granular soils. *J. Geotech. Geoenviron. Eng.* 140, 04013024.
- Amaya-Gomez, R., Ramírez-Camacho, J.G., Pastor, E., Casal, J., Munoz, F., 2018. Crater formation by the rupture of underground natural gas pipelines: a probabilistic-based model. *J. Nat. Gas Sci. Eng.* 54, 224–239.
- Argyropoulos, C.D., Markatos, N.C., 2015. Recent advances on the numerical modelling of turbulent flows. *Appl. Math. Model.* 39, 693–732.
- Bezaatpour, J., Fatehifar, E., Rasoulzadeh, A., 2020. CFD investigation of natural gas leakage and propagation from buried pipeline for anisotropic and partially saturated multilayer soil. *J. Clean. Prod.*, 123940.
- Biezma, M.V., Andrés, M.A., Agudo, D., Briz, E., 2020. Most fatal oil & gas pipeline accidents through history: a lessons learned approach. *Eng. Fail. Anal.* 110, 104446.
- Bonnaud, C., Cluzel, V., Corcoles, P., Dubois, J.-P., Louvet, V., Maury, M., Narbonne, A., Orefice, H., Perez, A., Ranty, J., Salim, R., Zeller, L.-M., Foissac, A., Poenou, J., 2018. Experimental study and modelling of the consequences of small leaks on buried transmission gas pipeline. *J. Loss Prev. Process. Ind.* 55, 303–312.
- Briefing, U.S., 2013. International Energy Outlook 2013. US Energy Information Administration.
- Cho, Y., Ulrich, B.A., Zimmerle, D.J., Smits, K.M., 2020. Estimating natural gas emissions from underground pipelines using surface concentration measurements. *Environ. Pollut.* 267, 115514.
- Cleaver, R., Halford, A., 2015. A model for the initial stages following the rupture of a natural gas transmission pipeline. *Process Saf. Environ. Protect.* 95, 202–214.
- Darteville, S., 2003. Numerical and Granulometric Approaches to Geophysical Granular Flows. MICHIGAN TECHNOLOGICAL UNIVERSITY.
- Deng, Y., Hou, H., Fang, L., Yuan, Q., Yu, B., Liang, Y., 2018. Numerical simulation on the dispersion of natural gas releases from a buried pipeline. *Heat Tran. Eng.* 39, 687–699.
- Ding, J., Gidaspow, D., 1990. A bubbling fluidization model using kinetic theory of granular flow. *AIChE J.* 36, 523–538.
- Ebrahimi-Moghadam, A., Farzaneh-Gord, M., Arabkoohsar, A., Moghadam, A.J., 2018. CFD analysis of natural gas emission from damaged pipelines: correlation development for leakage estimation. *J. Clean. Prod.* 199, 257–271.
- Ebrahimi-Moghadam, A., Farzaneh-Gord, M., Deymi-Dashtebayaz, M., 2016. Correlations for estimating natural gas leakage from above-ground and buried urban distribution pipelines. *J. Nat. Gas Sci. Eng.* 34, 185–196.
- Geng, Z., Li, X., Chen, G., Zhu, H., Jiang, S., 2021. Experimental and numerical study on gas release and dispersion from underwater soil. *Process Saf. Environ. Protect.* 149, 11–21.

- Gidaspow, D., Bezburuah, R., Ding, J., 1992. Hydrodynamics of circulating fluidized beds: kinetic theory approach, 7th Fluid. Conf. In: Illinois Inst. Of Tech. Dept. of Chemical Engineering, Chicago, IL (United States), pp. 75–82.
- Gryczka, O., Heinrich, S., Deen, N., van Sint Annaland, M., Kuipers, J., Jacob, M., Mörl, L., 2009. Characterization and CFD-modeling of the hydrodynamics of a prismatic spouted bed apparatus. *Chem. Eng. Sci.* 64, 3352–3375.
- Hibi, Y., Fujinawa, K., Nishizaki, S., Okamura, K., Tasaki, M., 2009. Multi-component migration in the gas phase of soil: comparison between results of experiments and simulation by dusty gas model. *Soils Found.* 49, 569–581.
- Hilme, M.I., Chandra, M.S., Karuppanan, S., Fadhl, M., Lias, M.R., 2013. Effects of different granular viscosity models on the bubbling fluidized bed - a numerical approach. *Appl. Mech. Mater.* 393, 857–862.
- Hosseini, S.H., Ahmadi, G., Olazar, M., 2013. CFD simulation of cylindrical spouted beds by the kinetic theory of granular flow. *Powder Technol.* 246, 303–316.
- Houssin-Agbomson, D., Blanchetière, G., McCollum, D., Saint-Macary, C., Mendes, R.F., Jamois, D., Barbalat, M., Foissac, A., Lubet, T., 2018. Consequences of a 12-mm diameter high pressure gas release on a buried pipeline. Experimental setup and results. *J. Loss Prev. Process. Ind.* 54, 183–189.
- Leis, B., Pimputkar, S., Ghadiali, N., 2002. Line Rupture and the Spacing of Parallel Lines. Battelle Memorial Institute.
- Link, J., Cuypers, L., Deen, N., Kuipers, J., 2005. Flow regimes in a spout–fluid bed: a combined experimental and simulation study. *Chem. Eng. Sci.* 60, 3425–3442.
- Link, J., Deen, N., Kuipers, J., Fan, X., Ingram, A., Parker, D., Wood, J., Seville, J., 2008. PEPT and discrete particle simulation study of spout–fluid bed regimes. *AIChE J.* 54, 1189–1202.
- Liu, C., Liao, Y., Liang, J., Cui, Z., Li, Y., 2021. Quantifying methane release and dispersion estimations for buried natural gas pipeline leakages. *Process Saf. Environ. Protect.* 146, 552–563.
- Lowesmith, B., Hankinson, G., 2013. Large scale experiments to study fires following the rupture of high pressure pipelines conveying natural gas and natural gas/hydrogen mixtures. *Process Saf. Environ. Protect.* 91, 101–111.
- Lun, C., Savage, S.B., Jeffrey, D., Chepurniy, N., 1984. Kinetic theories for granular flow: inelastic particles in Couette flow and slightly inelastic particles in a general flowfield. *J. Fluid Mech.* 140, 223–256.
- Lutostansky, E., Creitz, L., Jung, S., Schork, J., Worthington, D., Xu, Y., 2013. Modeling of underground hydrogen pipelines. *Process Saf. Prog.* 32, 212–216.
- Markatos, N.C., 2012. Dynamic computer modeling of environmental systems for decision making, risk assessment and design. *Asia Pac. J. Chem. Eng.* 7, 182–205.
- Massimilla, L., Volpicelli, G., Zenz, F., 1963. Flow of fluid-particle suspensions from liquid-fluidized beds. *Ind. Eng. Chem. Fundam.* 2, 194–199.
- Menter, F.R., 1994. Two-equation eddy-viscosity turbulence models for engineering applications. *AIAA J.* 32, 1598–1605.
- Niven, R.K., 2002. Physical insight into the Ergun and Wen & Yu equations for fluid flow in packed and fluidised beds. *Chem. Eng. Sci.* 57, 527–534.
- Okamoto, H., Gomi, Y., 2011. Empirical research on diffusion behavior of leaked gas in the ground. *J. Loss Prev. Process. Ind.* 24, 531–540.
- Okamoto, H., Gomi, Y., Akagi, H., 2014. Movement characteristics of hydrogen gas within the ground and its detection at ground surface. *J. Civil Eng. Sci.* 3, 49–66.
- Parvini, M., Gharagouzlou, E., 2015. Gas leakage consequence modeling for buried gas pipelines. *J. Loss Prev. Process. Ind.* 37, 110–118.
- Schaeffer, D.G., 1987. Instability in the evolution equations describing incompressible granular flow. *J. Differ. Equ.* 66, 19–50.
- Schiller, L., Naumann, A., 1935. A drag coefficient correlation. *Zeit. Ver. Deutsch. Ing.* 77, 318–320.
- Silva, E.P., Nele, M., e Melo, P.F.F., Könözy, L., 2016. Underground parallel pipelines domino effect: an analysis based on pipeline crater models and historical accidents. *J. Loss Prev. Process. Ind.* 43, 315–331.
- Soe, T.M., Khaing, S., 2017. Comparison of turbulence models for computational fluid dynamics simulation of wind flow on cluster of buildings in mandalay. *International Journal of Scientific and Research Publications* 7, 337–350.
- Soil, A.C.D.-o., Rock, 2017. Standard Practice for Classification of Soils for Engineering Purposes (Unified Soil Classification System) 1. ASTM international.
- Sun, Y., Cao, X., Liang, F., Bian, J., 2020. Investigation on underwater gas leakage and dispersion behaviors based on coupled Eulerian-Lagrangian CFD model. *Process Saf. Environ. Protect.* 136, 268–279.
- Sutkar, V.S., Deen, N.G., Kuipers, J., 2013. Spout fluidized beds: recent advances in experimental and numerical studies. *Chem. Eng. Sci.* 86, 124–136.
- Symlal, M., Rogers, W., O'Brien, T., 1993. MFX Documentation: Volume 1, Theory Guide. National Technical Information Service, Springfield, VA. DOE/METC-9411004, NTIS/DE9400087.
- Upadhyay, M., Kim, A., Kim, H., Lim, D., Lim, H., 2020. An assessment of drag models in eulerian–eulerian cfd simulation of gas–solid flow hydrodynamics in circulating fluidized bed riser. *ChemEngineering* 4, 37.
- Vianello, C., Maschio, G., 2014. Quantitative risk assessment of the Italian gas distribution network. *J. Loss Prev. Process. Ind.* 32, 5–17.
- Wakoh, H., Hirano, T., 1991. Diffusion of leaked flammable gas in soil. *J. Loss Prev. Process. Ind.* 4, 260–264.
- Wang, C., Li, Y., Teng, L., Gu, S., Hu, Q., Zhang, D., Ye, X., Wang, J., 2019. Experimental study on dispersion behavior during the leakage of high pressure CO₂ pipelines. *Exp. Therm. Fluid Sci.* 105, 77–84.
- Wilkening, H., Baraldi, D., 2007. CFD modelling of accidental hydrogen release from pipelines. *Int. J. Hydrogen Energy* 32, 2206–2215.
- Xinhong, L., Guoming, C., Renren, Z., Hongwei, Z., Jianmin, F., 2018. Simulation and assessment of underwater gas release and dispersion from subsea gas pipelines leak. *Process Saf. Environ. Protect.* 119, 46–57.
- Yan, Y., Dong, X., Li, J., 2015. Experimental study of methane diffusion in soil for an underground gas pipe leak. *J. Nat. Gas Sci. Eng.* 27, 82–89.
- Zakikhani, K., Nasiri, F., Zayed, T., 2020. A Review of failure prediction models for oil and gas pipelines. *J. Pipeline Syst. Eng. Pract.* 11, 03119001.
- Zhang, J., Tang, F., 2006. Prediction of flow regimes in spout-fluidized beds. *China Particul.* 4, 189–193.
- Zhang, Y., Weng, W.G., 2020. Bayesian Network Model for Buried Gas Pipeline Failure Analysis Caused by Corrosion and External Interference. *Reliability Engineering & System Safety*, p. 203.
- Zhao, J., Liu, G., Yin, X., Li, X., Gao, Z., Lu, H., 2021. Two-fluid simulation of a three-dimensional spout-fluid bed: flow structures, regimes, and insight into the mechanism of particle–particle momentum transfer. *Ind. Eng. Chem. Res.* 60, 7950–7965.
- Zhong, W., Zhang, M., Jin, B., Yuan, Z., 2007. Flow behaviors of a large spout-fluid bed at high pressure and temperature by 3D simulation with kinetic theory of granular flow. *Powder Technol.* 175, 90–103.
- Zhou, K., Nie, X., Wang, C., Wang, Y., Niu, H., 2021. Jet fires involving releases of gas and solid particle. *Process Saf. Environ. Protect.* 156, 196–208.